Supporting Information for “Induced Plant Defenses, Host-Pathogen Interactions, and Forest Insect Outbreaks”

Bret D. Elderd, Brian J. Rehill, Kyle Haynes, and Greg Dwyer

August 12, 2013

1 Details of Experimental Methods, and Additional Experimental Results

1.1 JA Application and Chemical Analyses

class of compound were calculated based on standard curves generated with oak tannins purified by a modification of the method of Hagerman and Butler (1980).

1.2 Results from Sample Collections in the Year Following JA Spray

Previous work showed that defoliation of red oak in one year can lead to hydrolyzable tannin induction in the following year (Hunter and Schultz 1993). We therefore collected a final set of samples from each branch in the season following our experiments, again at budburst. In the year following

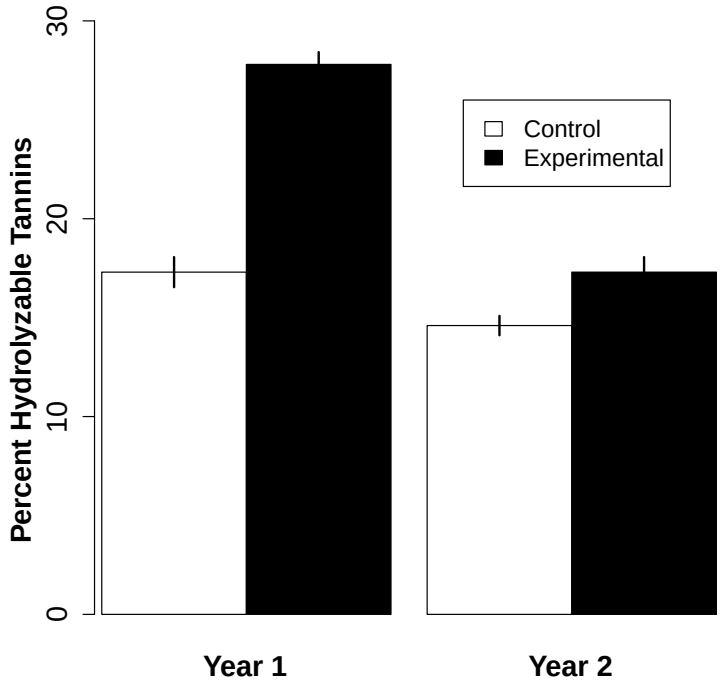

et al. 2012).

The initially uninfected larvae began feeding after leaves were fully expanded, which is when leaf chemistry ceases to change, so defoliation during the field experiment had no effect on hydrolyzable-tannin levels (D'Amico et al. 1998). Meanwhile, 25 uninfected larvae is a large enough number to provide reasonable statistical power, but it prevents starvation because 25 larvae per 40 leaves leads to defoliation levels of less than 50%. We further note that the density of initially uninfected larvae during a field transmission experiment has little to no effect on infection rates or induced defenses (D'Amico et al. 1998).

As in previous experiments (Dwyer et al. 2005), our protocol did not eliminate the effects of variability in infection risk, raising the question, what is the source of the variability? The answer is almost certainly stochastic fluctuations in infection risk within individuals over time, because such variability is equivalent to demographic stochasticity, and by using hundreds of insects, we greatly reduced the effects of demographic stochasticity. Instead the source appears to be heritable variation at loci that affect infection risk. In previous work, we showed that infection risk in gypsy moth larvae does indeed have a heritable component (Elderd et al. 2008), and because the larvae in the current study were all raised under the same conditions, the variability that we observed here was also probably heritable. In gypsy moths, heritable variation in infection risk is likely maintained by fluctuating natural selection, in combination with a fecundity cost of resistance (Elderd et al. 2008). We did not include selection in our models, however, because we wanted to explain the defoliation data with as simple a model as possible.

1.4 Analysis of Transmission Data

Because virus density was constant in our field experiment, and because the experiment was short enough that none of the initially uninfected larvae became infected and died during transmission, infection was the only process that occurred. This in turn meant that we could analyze our data using what is known in the stochastic processes literature as a "pure-death" model, which allows for the effects of small population size, so-called "demographic stochasticity" (Renshaw 1993). Because we used a total of 200 host insects in each experimental treatment (8 replicates $\times$ 25 larvae per replicate), the effects of demographic stochasticity were likely minimal, but it was nevertheless

important to allow for such effects (Dwyer et al. 2005; Elderd et al. 2008). The pure-death process predicts that the number of survivors per unit time follows a binomial distribution with a probability of survival that is a function of time and a rate parameter that can be fit to the data (Renshaw 1993). Also, because individuals vary in their risk of infection, we assume that the pure-death parameter, which is essentially the disease transmission rate, is drawn from a gamma distribution, with mean transmission rate $\bar{\nu}$ and coefficient of variation C.

Standard practice in analyzing mortality data is therefore to use a binomial distribution as a likelihood function McCullagh and Nelder (1989), and we thus used a binomial likelihood function

variance-inflation factor was very close to the ideal value of 1, our choice of a binomial distribution was clearly appropriate (Burnham and Anderson 2002). The best model thus explained essentially all of the variability in our data that was not simply due to low levels of demographic stochasticity.

An important point is that allowing variability C to approach 0 in a nonlinear transmission model yields a linear transmission model, and so the linear models were nested within the nonlinear models. This in turn meant that, when we fit a nonlinear transmission model to our data, it was possible for the best-fitting value of the variability parameter to be indistinguishable from 0, in which case the conclusion would be that the best-fitting model is instead linear. This happened for the models for which average transmission was the same for induced and control branches but variability was different, and for which both average transmission and variability were different for induced and control branches. In both of these cases, however, the best-fitting model assumed that transmission was linear on induced branches, and on control branches, strengthening our basic conclusion. Because the best-fitting versions of these two models reduced to simpler models, we did not include them in the AIC table in the main text.

It is also important to emphasize that when we fit a *a* model to the data, the fitting routine *a* estimate the variability parameter, and so in such cases it would not be possible for the routine to conclude that the best model is nonlinear. This is relevant because when we fit a model for which transmission was nonlinear for induced branches and linear for control branches, the fitting routine instead concluded that transmission was linear for both treatments. In the AIC table in the main text, we therefore did not include the model that assumed transmission was nonlinear on induced branches and linear on control branches, because it was effectively the same as the model for which transmission was assumed, from the beginning, to be linear for both treatments. As the table shows, however, the model for which transmission was linear for both treatments provided a very poor explanation for the data, again strengthening our basic conclusion.

An important part of our argument is that induction strongly affects variability C in particular. This conclusion is supported by our parameter estimates for the best model, which allows for differences in both average infection risk $\bar{\nu}$ and variability in infection risk C between induced and control branches. As Table S1 shows, the value of $\bar{\nu}$ on induced branches was moderately lower, reflecting slightly lower average infection risk on induced branches, as in a previous laboratory experiment (Hunter and Schultz 1993), but the value of C was lower, reflecting much lower variability in

Experiment	Treatment	Mean (95% C.I.)	C.V. (95% C.I.)
Field	Control	0.21 /day/m^2 (0.1 $0, 0.2$)	$0.$ ($0.$ $41, 1.$

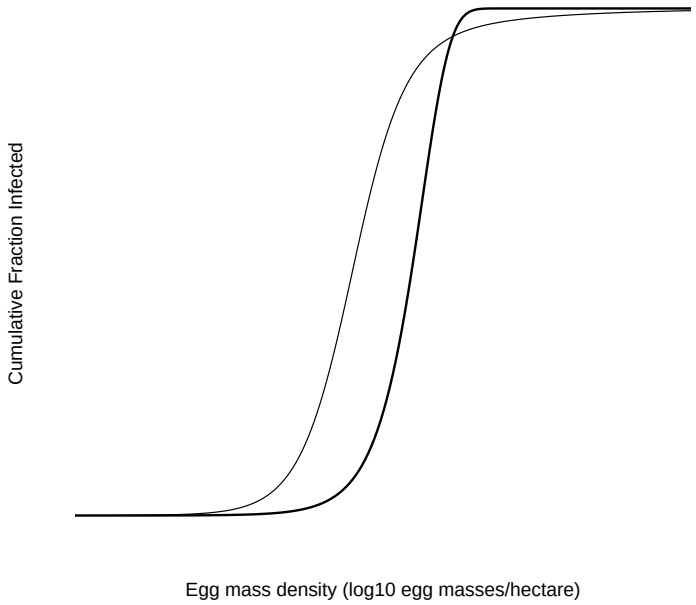

Figure S2: Effects of induction on epizootic intensity. The vertical axis is the cumulative fraction infected in a single epizootic, as calculated using the epizootic model in the main text. The "Induced" line is based on values of average transmission $\bar{\nu}$ and variability in transmission C estimated from induced foliage, while the "Non-induced" line is based on values estimated from non-induced foliage.

called “negative” density-dependence, but baculovirus infection rates in nature almost invariably rise with increasing host density, following “positive” density-dependence (Moreau et al. 2005; Woods and Elkinton 1987). Meanwhile, fig. S2 shows that a reduction in variability in infection risk causes the infection rate to rise more steeply with host density, which is a well-known result from epidemic theory (Anderson and May 1991). Theory therefore shows that a reduction in variability in infection risk due to induction should cause infection rates to rise very sharply with density, resolving the contradiction between the original experiment and data from naturally occurring virus epizootics in the field.

1.5 Feeding Trials and Dose-Response Bioassays

Once an insect has consumed some virus particles, infection risk depends only on the ability of the insect’s immune response to fight off the infection, but feeding behavior can alter the risk that the virus is consumed in the first place. In dose-response experiments, however, insects that do not consume the entire dose are discarded, and so infection rates depend only on the insect immune response, or on physiological factors that affect the immune response (Watanabe 1987). There are thus no effects of feeding behavior, even though feeding behavior is important in nature (Dwyer et al. 2005). Field transmission experiments thus have an advantage over laboratory dose-response experiments not just because field experiments allow for more natural conditions, but also because they allow for effects of both host behavior and (e)15(xpior)-249(and)-mmunesmmunedoss-35-6-2423vid82

consuming the virus and becoming infected, $P(I|C)$ as the probability of becoming infected given that the virus has been consumed, and $P(C)$ as the probability of consuming the virus. Following basic probability (Ross 1984), we can then write,

$$P(I, C) \qquad P(I|C)P(C). \tag{S3}$$

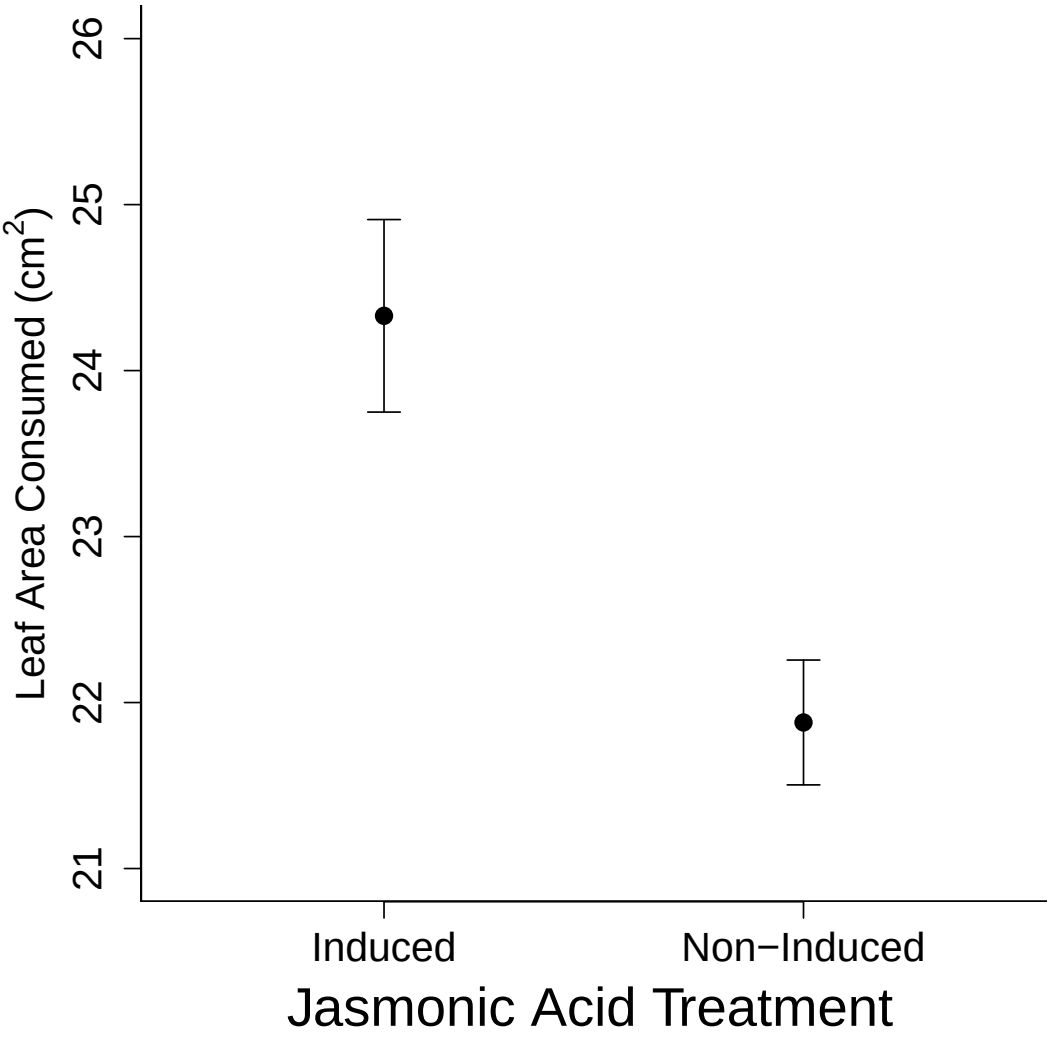

Figure S3: Effects of induction on gypsy moth feeding rate over 24 hours. Error bars indicate 1 standard error of the mean.

leads to increases in feeding rates, in turn altering infection risk. It therefore seems likely that the effects of induction on overall transmission were partly due to changes in feeding behavior.

In the dose-response experiment, we followed standard protocols by feeding larvae 3 μl of a solution of virus in dH_2O on leaf disks placed on top of agar squares in tightly sealed plastic cups in the laboratory (Dwyer et al. 2005; Hunter and Schultz 1993). Larvae that did not consume the entire leaf disk, and thus the entire dose of virus, were discarded. Control larvae were fed leaf disks with dH_2O alone. The data show that induction led to a lower infection rate at the lower dose, but infection rates were equal at the higher dose (Table S2).

	Dose (occlusion bodies)		
Treatment	0	9,000	30,000
Induced	0.00 ± 0.000	0.56 ± 0.109	0.97 ± 0.017
Non-Induced	0.00 ± 0.000	0.86 ± 0.050	0.97 ± 0.032

Table S2: Results of the dose-response bioassay, comparing the effects of induced and non-induced foliage on the probability of becoming infected given consumption of a particular dose of virus. Each value is the mean fraction infected, calculated across 6 replicates, plus or minus 1 standard error of the mean. Within a replicate, leaf disks were all from the same tree. Each replicate included 11-14 larvae. Out of 250 individuals in virus-control treatments, all of which were fed leaf disks in combination with dH_2O, none became infected.

The standard method of analyzing this type of data is to use generalized linear modeling to fit a logistic distribution to the data, using the so-called "logit transform" (Collett 2003). Under this transform, our model for the dose-response data is,

$$, \quad \left(\frac{1 - \ _i}{\ _i}\right) \qquad \beta_0 + \beta_1, \quad _{10} D_i. \tag{S4}$$

Here, $_i$ is the fraction infected at dose D_i, and β_0 and β_1 are parameters that are fit to the data. We fit versions of this model to the data under different assumptions about the effects of induction on the model parameters β_0 and β_1. If there were effects of induction, then in the best model either β_0 or β_1

Table S3: AIC analysis of bioassay data. The best model is in bold-face.

Model	AIC_c	ΔAIC_c	AIC_c weights

however, similar field experiments have not been carried out, and apparently as a consequence the literature on baculoviruses often invokes virus survival through covert infections, which are assumed to be activated by stress at some time after infection, due to unidentified stressors (Il'inykh and Ul'yanova 2005). Although covert infections have in fact been detected in some species of insects (Burden et al. 2003), whether or not such infections play a role in transmission in the field is debatable (see Fuller et al. (2012) for a brief review). Moreover, for gypsy moths in particular, surface-disinfection of egg masses, which we used in all of our experiments, is extremely effective at eliminating vertical transmission (Doane 1969), as it is in many other insects (Kukan 1999). For this reason, reports of vertical transmission through the activation of covert infections can often be more parsimoniously explained by a lack of surface-disinfection (Myers et al. 2000). It therefore seems likely that covert infections play only a small role in virus survival in the gypsy moth, and possibly in many other insects as well. In our model, we thus included only environmental reservoirs and surface contamination of egg masses as mechanisms of virus survival between host generations.

It is nevertheless worth pointing out that in fact our model may be adequate to describe the effects of covert infections as well. The crucial assumption is simply that some fraction of infections from previous generations leads to new infections in the current generation. As long as this fraction does not vary with insect density, and as along as such infections are either rare or occur mostly at the beginning of the larval season, our model may provide an accurate description of the effects of covert infections.

2.2 Re-scaling and Estimating Model Parameters

As we mentioned in the main text, we used the temporal model to develop a preliminary understanding of the effects of induction on insect outbreaks, and to generate preliminary estimates of some parameters. Before fitting model parameters to data, however, it was important to identify parameters that have identical effects on the model's predictions, as the values of such parameters will be perfectly correlated and thus statistically non-identifiable. We therefore first re-scaled the model. Because the infection rate depends on the epidemic model in the main text, we re-scaled both the year-to-year state variables N_n, $_n$, and D_n, and the epidemic state variables $(\ )$, $E_i(\ )$, and $I(\ )$,

$\mathbb{N}$

as follows:

$$(\ ) \equiv \bar{\nu} \quad (\ ), \tag{S7}$$

$$E_i(\ ) \equiv \bar{\nu}\, E_i(\ ), \tag{S8}$$

$$P(\ ) \equiv \bar{\nu}\, P(\ ), \tag{S9}$$

$$N_n \equiv \bar{\nu}\, N_n, \tag{S10}$$

$$_n \equiv \bar{\nu}\rho \quad _n, \tag{S11}$$

$$D_n \equiv \psi\, D_n. \tag{S12}$$

Allowing for this re-scaling, the epizootic model becomes:

$$— \qquad - \ P\left[\frac{(\ )}{(0)}\right]^{C_r^2}, \tag{S13}$$

$$\underline{E_1} \qquad P\left[\frac{(\ )}{(0)}\right]^{C_r^2} - \quad \delta E_1, \tag{S14}$$

$$\underline{E_i} \qquad \delta E_{i-1} - \quad \delta E_i, \qquad 2, \ldots \quad , \tag{S15}$$

$$\underline{P} \qquad \delta E_m - \mu P. \tag{S16}$$

Note that variability varies from generation to generation because of changes in induced defenses, such that $C_n \quad C_0 \quad \left(-(D_n + D_0)\right)$. The multi-generation model is then:

$$N_{n+1} \qquad \lambda \epsilon_n N_n \left(1 - \ (N_n, \ _n, D_n)\right) \left(1 -

μ 0.3 /day (Fuller et al. 2012). The parameters C_0, α, β and D_0 in contrast are related to the dynamics of hydrolyzable tannins, and consequently have not been previously measured, while the pathogen over-wintering parameters ϕ and γ are not well known. To produce preliminary estimates of these six parameters, we therefore followed Kendall et al. (1999) in fitting the period and the amplitude of the model cycles to the corresponding values from a combination of our experimental data and observations of gypsy moth populations in nature. This required that we run the model repeatedly to find sets of parameters for which the model output matched the data.

To understand this fitting procedure, note that hydrolyzable tannins can only be measured as a fraction of a sample's dry weight, because the total dry weight of leaf material in the forest is unknown. In fitting the model to the data, we therefore calculated the amplitude of change in the log of the hydrolyzable tannin concentration, $_{10}(D_n + D_0)$, so that total dry weight fell out of the calculation as a scaling constant (note that this would not have been true if we had scaled away the baseline variability C_0). In our data, the difference in, $_{10}$ of hydrolyzable tannin concentrations before and after induction was 0.1 ± 0.02 . Meanwhile, gypsy moth populations cycle with a period of 5-10 years, and with an amplitude of roughly 3-5 orders of magnitude (Williams et al. 1991). We thus searched for values of α, β, D_0, ϕ, and γ for which the amplitude of fluctuations in the host population was at least 3 orders of magnitude, the amplitude of fluctuations in the induced defense was within about 0.0 of 0.1 , and the cycle period was at least 5 years. We then ran the model for 200 generations, discarding the first 50 generations to avoid transients, and we calculated the average amplitude and the period for the remaining 150 generations. To reduce the computational burden, we temporarily eliminated stochasticity by setting the standard deviation of the random variate σ 0.

Figure S4: Dynamics of the temporal model. Parameter values are: scaled induction response α 2. , scaled induction half-saturation constant β 100, baseline heterogenity C_0 0.04, scaled constitutive defense level D_0 3, long-term virus over-wintering γ 0.2, reproductive rate λ 4. , maximum predation rate 0. , density at which predation is maximized 0.14 m^{-2}, virus decay rate μ 0.3 /day. The average amplitude of the cycles in the induced defense is 0.1 , and the average amplitude of the cycles in the host population is . orders of magnitude.

Figure S5: As in fig. S4, except here α $0.$, so that increases in the induced defenses are weak. The cycles therefore damp out.

This occurs because, for this value of α, induction is very weak, so the induced defense never rises high enough to allow for the severe density-dependence that drives outbreaks. The temporal model therefore suggests that induced defenses play a key role in driving gypsy moth outbreaks in nature. The comparison of the spatial model to the defoliation data neverthless provides a more convincing test of the model, and so the spatial model is the focus of the main text.

In figures (S4) and (S5), and in the figures in the main text, we include panels showing fluctuations in the fraction of trees defoliated. To generate those panels, we translated the model prediction of host population density into a fraction defoliated, using a statistical model and associated parameters from the literature, such that the statistical model parameters had been estimated by correlating defoliation levels with egg densities (Williams et al. 1991). Note that, in the non-dimensionalized version of the model, host density is scaled by the average transmission rate $\bar{\nu}$, which in our experiments is expressed in terms of /day/m^2 (in the model equations, the m^2 unit balances the units on infectious cadavers, which are in terms of /m^2). Once we converted from units of m^2 to units of acres, we therefore still had $\bar{\nu}$ as a free parameter. The value of this parameter is ultimately of little interest to our results, but for the sake of completeness we note that we achieved a good fit to the oak-hickory defoliation data for a value of $\bar{\nu}$ $0.$ /day/m^2, which is well within the 95% confi-

Here $_{q;r}$ is the distance between patch and patch , such that ω controls the degree to which dispersal declines with increasing distance from patch to patch , while κ is a scaling constant that ensures that the fraction of individuals dispersing sums to 1. For dispersal by larval ballooning, we instead used a Gaussian kernel, because it fits the ballooning data better.

Dispersal on automobiles typically occurs when females lay their egg masses on a vehicle. Such egg masses, however, comprise only a small fraction of the total, and so in the model we assumed that a fraction ζ of each population disperses between patches, after the epizootic, when the egg masses are laid (Liebhold et al. 1992). Based on previous work, we set ζ 10^{-5} and ω $0.$ km^{-1}, respectively (Abbott and Dwyer 2008). The transported egg masses then hatch in their new patch the following spring, at which time larvae disperse following a normal dispersal kernel, with an average dispersal distance of 1 . m, as estimated from data on ballooning larvae (Hunter and Elkinton 2000).

We then set the spatial scale of the model forest to be 25 km on a side, for a total of 625 km^2 of forest, a typical forest size in the range of the gypsy moth in North America. We assumed that weather stochasticity was the same across grid cells, ensuring the high level of spatial synchrony typical of gypsy moth populations at this scale Peltonen et al. (2002). Because the defoliation data to which we compared the model were collected in areas that had been colonized by the insect decades earlier Johnson et al. (2006), we assumed that the insect had already infested the entire forest.

At the beginning of each realization of the model, the probability that the tree genera at each location were inducible was determined by drawing a $(0, 1)$ random variate, such that if this random variate was less than the overall fraction inducible , the location was strongly inducible, otherwise it was weakly inducible. Next, following the way in which the defoliation data were summarized (Johnson et al. 2005), we averaged the fraction defoliated across spatial locations, to produce a single time series of defoliation for each realization of the model. To produce power spectra, we used only the last 50 years of each 100-year simulation, roughly matching the time lag between the introduction of the gypsy moth and when the data were collected, and we averaged the spectra across 100 realizations. Power spectra were calculated using the `spectrum` function in the R programming language (R Development Core Team 2009).

An important point is that power spectra can have minor peaks at integral divisors of the period

associated with a major peak, simply because of the non-sinusoidal character of the data (Chatfield 2003). For our model, however, when the forest is 43% inducible, the peaks of the power spectrum occur at 9 years and about 4.9 years, confirming that the sub-harmonic in the model is not a statistical artifact. The occurrence of non-sinusoidal features in most data sets is also a good reason to combine spectral analysis with visual inspection of the time series being analyzed (Chatfield 2003). In both this document and in the main text, we therefore base our assessment of the fit of the spatial model partly on a visual comparison of model time series to data time series.

Figure S6: 10 realizations of the spatial model, with 43% of the forest inducible, corresponding to oak-hickory forests. Filled circles identify time periods during which model output provides a near-exact visual match to the defoliation data.

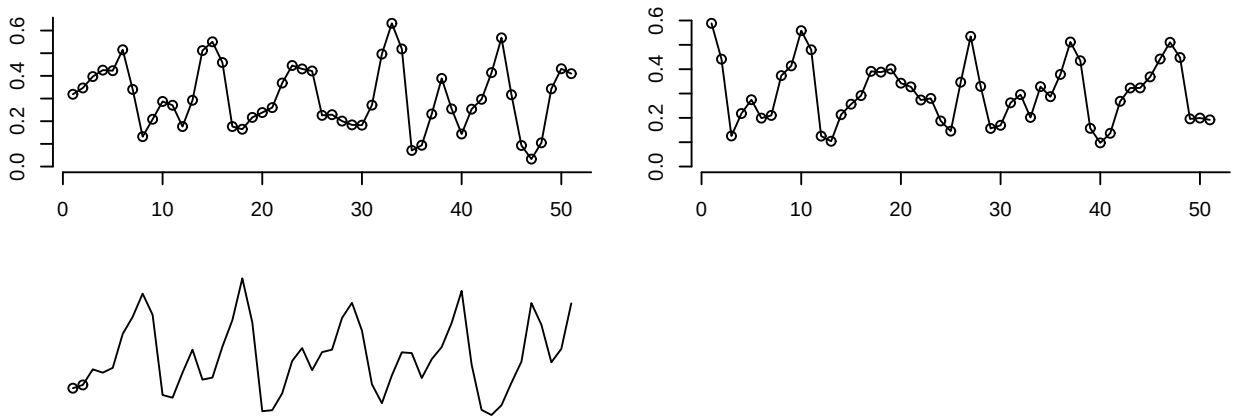

Figure S7: 10 additional realizations of the spatial model, as in fig. S6.

Figure S9: 10 additional realizations of the spatial model, as in fig. S6.

Figure S12: 10 additional realizations of the spatial model, as in fig. S11.

Figure S13: 10 additional realizations of the spatial model, as in fig. S11.

Figure S14: 10 additional realizations of the spatial model, as in fig. S6.

Figure S15: 10 additional realizations of the spatial model, as in fig. S6.

α much above the baseline values instead caused the model to do a poor job of fitting the oak-pine data. In short, the model shows realistic output even if the values of α are somewhat lower than our best-fit values. We therefore argue that our results are not particularly sensitive to changes in the value of α.

Increasing α also had the effect of increasing the fraction of realizations that produced at least two alternations of mild and severe outbreaks, as in the defoliation data. The effect is modest, however, such that for $\alpha \quad 4$ the fraction was 0.4, instead of the 0.5 produced by $\alpha \quad$. The value of α on non-induced foliage also had a modest effect on this fraction, such that $\alpha \quad 1$ gives 0.5, $\alpha \quad 0.$ gives 0.4, and $\alpha \quad 0.2$ gives 0.2. Substantially higher values of α on either inducible or non-inducible foliage gave a poor fit to the oak-pine data. A more general point is that, because we fit the values of α for the spatial model to the defoliation data, the results of the spatial model are not dependent on the experimental data. This is the basis of our claim in the Discussion that the experimental and observational data provide independent lines of argument.

The reason why individual trajectories in simulated oak-hickory forests do not always match the data has to do with the effects of stochasticity on outbreaks. Weather stochasticity is strongly synchronizing in the model, as it is in nature (Peltonen et al. 2002), but the synchronization is specific to either inducible or non-inducible trees. To illustrate this effect, in fig. S16, we show a realization for which severe and mild outbreaks alternate for the entire time series (upper panel),

Figure S16: The upper panel shows a single realization of the model, for a case in which the model produces a strict alternation of severe and moderate cycles, as in the defoliation data for oak-hickory forests. The lower panel shows time series for all of the inducible locations and all of the non-inducible locations, such that the data for each location are plotted separately. The lines for the inducible locations are thus all plotted exactly on top of each other, as are the lines for the non-inducible locations. The panel therefore shows that the respective tree types, inducible and non-inducible, have their own synchronized cycles.

locations of inducible and non-inducible trees, in other realizations the peaks of these distinct cycles are not always in synchrony, and in such cases the model trajectory will not show a strict alternation of mild and severe outbreaks. As we mentioned in the main text, the lack of an obvious sub-harmonic in more recent defoliation data may reflect these effects (Johnson et al. 2006), although it may also reflect the effects of the more recently introduced fungal pathogen *E a a a a a* (Dwyer et al. 2004). We reiterate, however, that a sub-harmonic never occurs by chance in model trajectories from oak-pine forests because inducible trees represent such a small proportion of oak-pine forests.

2.3.2 Modifications of the basic model

In the interests of parsimony, in the main text we present the simplest model that can explain the data, but here we consider alternative model structures, to show that our results are robust to changes in assumptions about the effects of induction. First, in the main text we used a model in which induction affects only variability in transmission, rather than average transmission, because induction had much stronger effects on variability in transmission than it had on average transmission. More generally, however, average transmission is strongly dependent on insect feeding and movement behavior, which are in turn affected by leaf toughness and leaf architecture (Dwyer et al. 2005), whereas variability in transmission is scale-independent and therefore more likely to be robust to differences in leaf characteristics. Because the effects of leaf characteristics on transmission are poorly understood, and because the model that leaves out such effects is more parsimonious, we assumed that differences in host-tree genera only affect variability in transmission. To test whether this assumption affected our conclusions, we also considered a model in which transmission rate declines exponentially with increasing levels of the induced defense, with rate parameter η, much as variability declines exponentially with defenses in the main model (unlike the corresponding parameter ψ for the change in variability, this parameter cannot be scaled away). We then adjusted η to find a value that gave an amplitude of fluctuation of $_{10}(\bar{\nu})$ that included the range seen in our experiments ($\eta \quad 0.1$ gave a good fit to the experimental amplitude of 0.55). As figure (S17)

=0euuuTJ-1d[]-3(seen)d6((San)-38u(0San)bheaf-274(the)-323()d thethes-228(no)-227(ot3(f)-3a227(c)1-38(

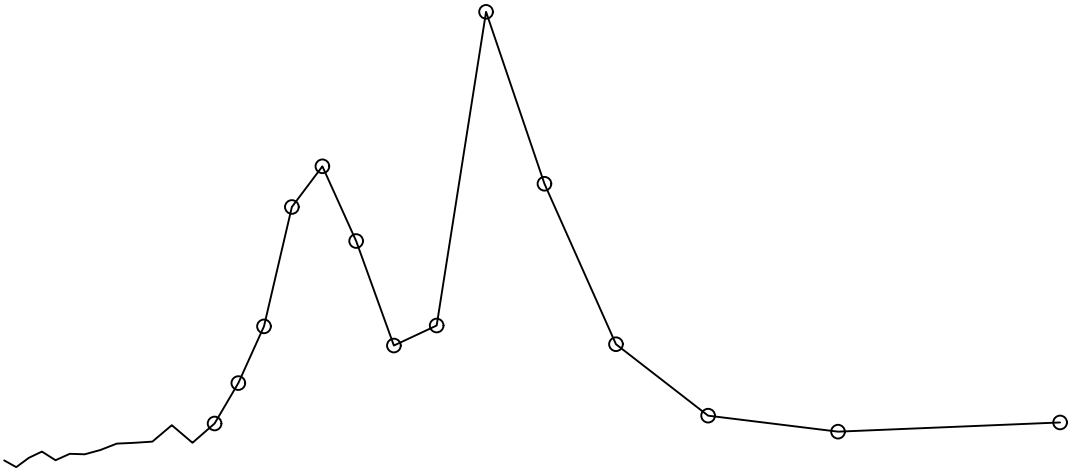

Figure S17: Effects of tannin-dependent average transmission on power spectra of the model output. As in the main text, induced defenses lower variability in infection risk C, but in this case they also lower average infection risk $\bar{\nu}$.

As we mentioned in the main text, our basic results are robust to a moderate reduction in the insect's reproductive rate on non-oaks (fig. S18). In this case, the sub-harmonic in the power spec-

Figure S18: Effects of a 25% reduction in host reproductive rate on non-oak locations on the power spectrum of the defoliation time series. Note that there is an increase in the super-harmonic in oak-pine forests. In spite of the superharmonic, however, the time series of defoliation in oak-pine forests do not show obvious alternation of severe and moderate outbreaks (not shown).

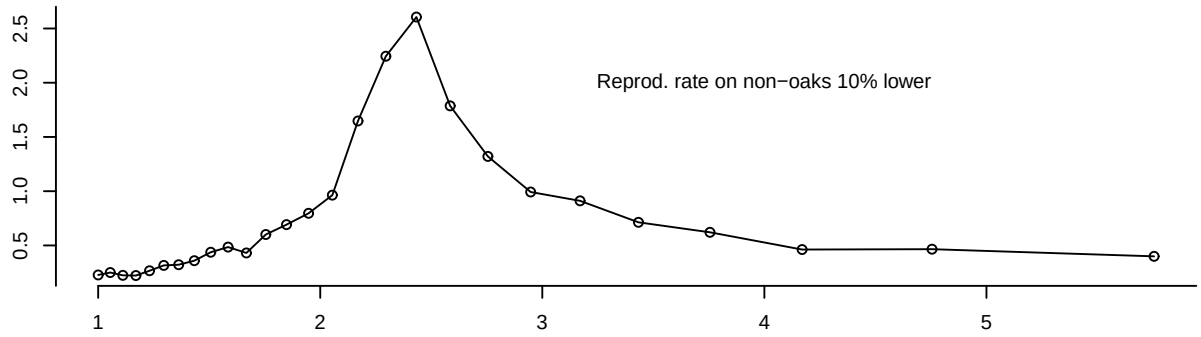

Figure S19: Effects of reductions in host reproductive rate on the power spectrum when there is no variability in inducibility across spatial locations. In all 3 cases, 43% of spatial locations are oaks, corresponding to oak-hickory forests. Irrespective of the reduction in the reproductive rate on non-oaks, there is no meaningful sub-harmonic.

densities on non-oaks in the following generation. The data thus suggest that, at least some of the time, densities on non-oaks are indeed higher than on oaks, as our model predicts. This effect occurs in the model because virus epizootics are more severe on oaks, but an alternative explanation for the pattern in nature is that larvae may move away from oaks near the end of the larval season (Lechowicz and Jobin 1983; Mauffette and Lechowicz 1984; Rossiter 1987). Unfortunately, however, there are no data indicating which explanation is correct.

Moreover, it is not possible to allow for tree-species-specific movement rates in our model, because of a lack of tree-species-specific movement data. Testing whether such movement would alter our model results is therefore also not possible. Our overall argument is thus that, given the available data, our model provides the best explanation for differences in gypsy-moth cycles between forest types.

A final point is that we also tried different numbers of grid points, ranging from a $\times$ grid to a $2\ 0 \times 2\ 0$ grid, with the model results presented here based on a 100×100 grid. As the number of grid points increased beyond $1\ 0 \times 1\ 0$, realizations that produced exactly alternating high and low defoliation levels became somewhat less likely, although the power spectra were unchanged. This effect suggests that at least mild patchiness in inducibility is necessary for alternating peaks, but the effect is rather weak. Further research is clearly needed to understand such effects.

References

ABBOTT, K. C. AND DWYER, G. 2008. Using mechanistic models to understand synchrony in forest insect populations: the North American gypsy moth as a case study. American Naturalist 172:613–624.

ANDERSON, R. M. AND MAY, R. M. 1991. Infectious diseases of humans: Dynamics and control. Oxford University Press.

BATE-SMITH, E. C. 1975. Phytochemistry of proanthocyanidins. Phytochemistry 14:1107–1113.

BURDEN, J., NIXON, C., HODGKINSON, A., POSSEE, R., SAIT, S., KING, L., AND HAILS, R. 2003. Covert infections as a mechanism for long-term persistence of baculoviruses. Ecology Letters 6:524–531.

BURNHAM, K.

DWYER, G., FIRESTONE, J., AND STEVENS, T. E. 2005. Should models of disease dynamics in herbivorous insects include the effects of variability in host-plant foliage quality? The American Naturalist 165:16–31.

ELDERD, B., DUSHOFF, J., AND DWYER, G. 2008. Does natural selection on disease susceptibility play a role in insect outbreaks? The American Naturalist 172:829–842.

ELKINTON, J. S., HEALY, W. M., BUONACCORSI, J. P., BOETTNER, G. H., HAZZARD, A. M., SMITH, H. R., AND LIEBHOLD, A. M. 1996. Interactions among gypsy moths, white-footed mice, and acorns. Ecology 77:2332–2342.

EVANS, M., HASTINGS, N. A. J., AND PEACOCK, B. 1993. Statistical Distributions, Second Edition. Wiley-Interscience.

FARAWAY, J. 2006. Extending the linear model with R: Generalized linear, mixed effects and nonparametric regression models. Chapman & Hall/CRC.

FULLER, E., ELDERD, B. D., AND DWYER, G. 2012. Pathogen Persistence in the Environment and Insect-Baculovirus Interactions: Disease-Density Thresholds, Epidemic Burnout, and Insect Outbreaks. American Naturalist 179:E70–E96.

GROVE, M. J. AND HOOVER, K. 2007. Intrastadial developmental resistance of third instar gypsy moths (*L a a a* l.) to *L. a* nucleopolyhedrovirus. Biological Control 40:355–361.

HAGERMAN, A. E. AND BUTLER, L. G. 1980. Condensed tannin purification andT2

IL'INYKH, A. AND UL'YANOVA, E. 2005. Latency of baculoviruses. Biology Bulletin 32:496–502.

JOHNSON, D., LIEBHOLD, A., AND BJORNSTAD, O. 2006. Geographical variation in the periodicity of gypsy moth outbreaks. Ecography 29:367–374.

JOHNSON, D. M., LIEBHOLD, A. M., AND BJORNSTAD, O. N. 2005. Circumpolar variation in periodicity and synchrony among gypsy moth populations. Journal of Animal Ecology 74:882–892.

JONES, C., OSTFELD, R., RICHARD, M., SCHAUBER, E., AND WOLFF, J. 1998. Chain reactions linking acorns to gypsy moth outbreaks and Lyme disease risk. Science 279:1023–1026.

KEATING, S. T., MCCARTHY, W. J., AND YENDOL, W. G. 1989. Gypsy moth (*L a a a*) larval susceptibility to a bacuiovirus affected by selected nutrients, hydrogen ions (pH), and plant allelochemicals in artificial diets. Journal of Invertebrate Pathology 54:165–174.

KENDALL, B. E., BRIGGS, C. J., MURDOCH, W. W., T

RENSHAW, E. 1993. Modelling Biological Populations in Space and Time. Cambridge University Press.

ROSS, S. M. 1984. A first course in probability. Macmillan.

ROSSITER, M. C. 1987. Use of a secondary host by non-outbreak populations of the gypsy moth. Ecology 68:857–868.

SCHULTZ, J. AND BALDWIN, I. T. 1982. Oak leaf quality declines in response to defoliation by gypsy moth larvae. Science 217:149–150.

WATANABE, H. 1987. The host population, pp. 71–112. In J. Fuxa and Y. Tanada (eds.), Epizootiology of insect diseases. Wiley: New York.

WILLIAMS, D., FUESTER, R., METTERHOUSE, W., BALAAM, R., BULLOCK, R., AND RJ, C. 1991. Oak defoliation and population-density relationships for the gypsy-moth (Lepidoptera:Lymantriidae). Journal of Economic Entomology 84:1508–1514.

WOODS, S. A. AND ELKINTON, J. S. 1987. Bimodal patterns of mortality from nuclear polyhedrosis-virus in gypsy-moth (*L a a- a*) populations. Journal Of Invertebrate Pathology 50:151–157.